Demonstration of Spectrally Resolved X-Ray Scattering in Dense Plasmas

S. H. Glenzer, G. Gregori, R. W. Lee, F. J. Rogers, S. W. Pollaine, and O. L. Landen

L-399, Lawrence Livermore National Laboratory, University of California, P.O. Box 808, Livermore, California 94551, USA

(Received 10 October 2002; published 2 May 2003)

We present the first spectrally resolved x-ray scattering measurements from solid-density plasmas. The scattering spectra show the broadened Compton down-shifted feature allowing us to determine the electron temperature and density with high accuracy. In the low temperature limit, our data indicate that the ionization balance reflects the electrons in the conduction band consistent with calculations that include quantum mechanical corrections to the interaction potential.

DOI: 10.1103/PhysRevLett.90.175002 PACS numbers: 52.35.Fp, 52.25.Os, 52.38.–r, 52.50.Jm

In modern physics, scattering experiments have been used extensively to obtain insight into the structure and the state of matter. We have therefore developed a novel x-ray scattering technique to provide independent tests of the microscopic models of dense matter for material properties such as the opacity, equation of state, or the conductivity. Thomson scattering with optical lasers [1,2] was demonstrated in low-density laboratory plasmas allowing accurate measurements of the plasma temperature and density by observing the scattering of an intense light source by the electrons [3] of the plasma. In the simplest scattering limit, the scattered photons are Doppler shifted by the thermal motion of the electrons in the plasma, therefore providing a measurement of the electron velocity distribution. For example, Thomson scattering is being applied in low-density magnetically confined fusion research plasmas [4] and, more recently, in inertial confinement fusion hohlraums where it provides accurate measurements of the electron temperature, ion temperature, ionization state, density, and flow velocity [5]. However, accessing solid-density or superdense plasma states requires hard x-ray probes [6,7] because optical probe lasers propagate efficiently only in underdense plasmas with electron densities of $n_e \leq 10^{21}$ cm^{-3} and not at all for $n_e > 10^{22}$ cm^{-3}. Here, we demonstrate that, by using an intense source of 4.75 keV x rays, we access the solid-density and superdense plasma regime that is of great interest in inertial confinement fusion, astrophysics, and warm dense matter research.

We employed the 30-kJ Omega laser facility [8] to produce solid-density plasmas close to the Fermi degenerate state that are fundamental states of matter occurring in high energy density laboratory experiments where laser or particle beams interact with solids. Figure 1(a) shows an example of a target consisting of a solid beryllium cylinder coated with 1 μm thick rhodium, Au shields, and a 2 μm thick annular titanium coating on the shields. To heat the beryllium homogeneously and isochorically to temperatures of 50 eV, we irradiate the rhodium directly with 15 kJ of 351-nm laser light in a 1-ns long square pulse by using 30 laser beams. Approximately 5%–10% of the laser energy is converted into Rh L-shell emission with photon energies in the range of 2.7 keV $< E <$ 3.4 keV. These x rays are absorbed by the beryllium with an absorption length matched to the cylinder radius (600 μm diameter, 750 μm long, with two counterbored ends: 100 μm deep and 400 μm diameter to avoid cold ends). Radiation-hydrodynamic simulations indicate that heating by these x rays for the duration of 1 ns results in a homogeneously heated solid-density plasma across the inner 400-μm diameter of the Be cylinder, with densities of $(2–3) \times 10^{23}$ cm^{-3} and temperatures of the order of 30 eV [cf. Fig. 1(b)].

The interior of this plasma state is probed with multi-keV x rays produced by a second laser plasma. For this purpose, the 2 μm thick titanium foil that was coated on the Au shields at a distance of $\sim$1 mm from the Be is irradiated with 7 kJ of 351 nm laser light delivered by 15 beams in a 1 ns square pulse. These beams are delayed by 1 ns with respect to the 30 heater beams so that the Be plasma is probed when the plasma temperature is homogeneous and maximized. At this time, the majority of the Be plasma has not expanded and is still at solid densities as indicated by simulations, and as observed by gated x-ray images at $t = 1.5$ ns [cf. Fig. 1(c)]. The 4.75 keV He–α resonance line emission from heliumlike titanium provides the narrow ($\Delta\lambda/\lambda < 0.005$) line required for spectrally resolved x-ray scattering.

The 4.75 keV x rays are scattered and absorbed in the high density Be plasma. We observe the scattered radiation in near backscattering geometry ($\theta \simeq 125°$) through a 400 μm diameter diagnostic hole in the center of the large Au shield. A near backscattering geometry has been chosen to maximize observable frequency shifts and to minimize effects of k-vector smearing due to finite probe and collection solid angles. Here k, the scattered wave number, is defined as the difference between the wave number of incident and the scattered x rays. The 5 mm large Au shields are attached on the far end of the Be cylinder to avoid a direct view of the Ti and Rh laser plasmas by the detector. Moreover, a Au shield is mounted to the target stalk to avoid x-ray scattering from the low-Z material in the stalk. The shields and the 400 μm diameter diagnostic hole assure that the detector

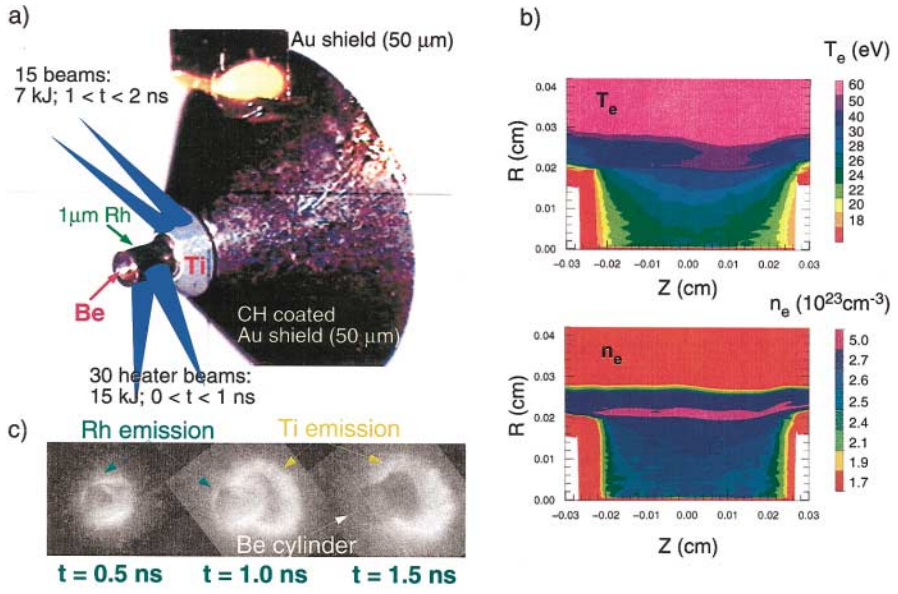

FIG. 1 (color). (a) Be target before it is heated by x rays from a Rh plasma produced by 30 laser beams. The annular titanium foil on the Au conical shield is heated by 15 beams providing the 4.75 keV line which is scattered from the Be plasma. The scattered x rays are observed through a hole in the center of the Au shield. (b) LASNEX calculation of the temperature and density of the plasma at $t = 1.3$ ns. (c) Gated x-ray images ($E > 2$ keV) showing the heating of the Rh foil at $t = 0.5$ ns, the onset of the titanium emission at $t = 1$ ns, and only the titanium emission at $t = 1.5$ ns close to when the x-ray scattering spectra are measured.

observes only the central homogeneously heated 400 μm wide and 500 μm long Be plasma.

By spectrally resolving the scattered radiation, we can discriminate between the elastic (Rayleigh) and the inelastic (Compton) scattering components, therefore measuring the electron temperature and density of the solid-density plasmas. We relay and spectrally disperse the scattered photons onto a gated framing camera by a high efficiency Bragg crystal (graphite) [9] operated in the mosaic focusing mode [10] providing a spectral resolution of $\Delta\lambda/\lambda \approx 0.003$. The fraction of scattered photons is substantial. For $n_e = 2 \times 10^{23}$ cm^{-3}, the Thomson scattering cross section of $\sigma_{TS} = 6.6 \times 10^{-25}$ cm^2, and a path length $x = 0.1$ cm, the fraction scattered is $n_e \sigma x = 0.01$, close to the maximum desirable for avoiding multiple scattering. Coupled with a source solid angle of 0.1 sr, the scattered fraction is 10^{-4}, which is substantially larger than that available for visible Thomson scattering at lower densities. For this experiment, the number of detected scattered photons has been estimated at 10^5, sufficient to yield high quality data on a single shot.

Figure 2(a) shows the x-ray scattering data from the heated beryllium plasma. Figures 2(b) and 2(c) show spectra measured by scattering from the cold (i.e., not heated) Be cylinder and by directly observing emission from a Ti disk plasma, respectively. The scattering spectra show peaks at 4.75 and 4.92 keV where the Ti plasma emits the strong He–α and Ly–α resonance lines as shown in Fig. 2(c) and which undergo elastic Rayleigh scattering by the Be. In addition, we observe the inelastic scattering component of both Ti lines on the red wing of the elastic components. These wings are the Compton down-shifted lines [11,12], that are broadened due to the thermal motion of the electrons [13]. Additional broadening is clearly observable when comparing the spectrum from the heated beryllium plasma [Fig. 2(a)] with the spectrum from the cold Be [Fig. 2(b)], and the spectral profile provides the electron temperature of the plasma with high accuracy.

Figure 3 shows the x-ray scattering spectra together with theoretical fits of the line shape using the random phase approximation (RPA) [14]. The fits take into account the probe radiation bandwidth and the spectral resolution of the Bragg crystal detector. The RPA

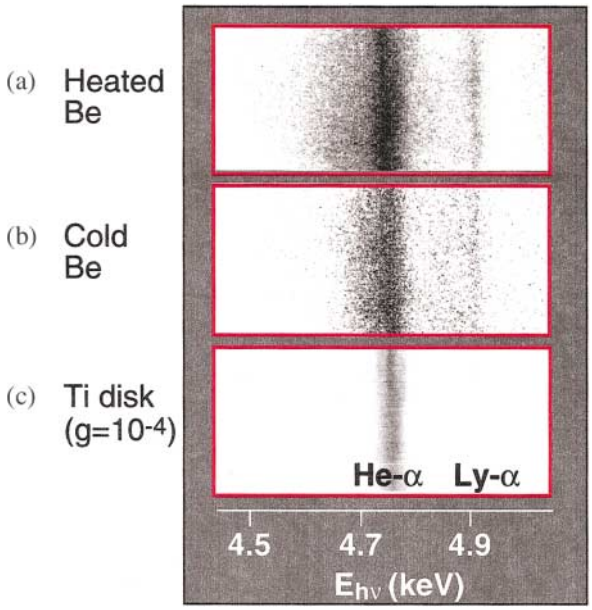

FIG. 2 (color). (a) Experimental x-ray scattering spectra from the isochorically heated Be plasma, and (b) from the cold beryllium. (c) Also shown is a spectrum measuring the direct emission from a Ti laser plasma with a reduced gain of the microchannel plate detector of 10^{-4}. These measurements were performed with a gate window of 0.4 ns at $t = 1.3$ ns, i.e., 0.3 ns after the heater beams turn off.

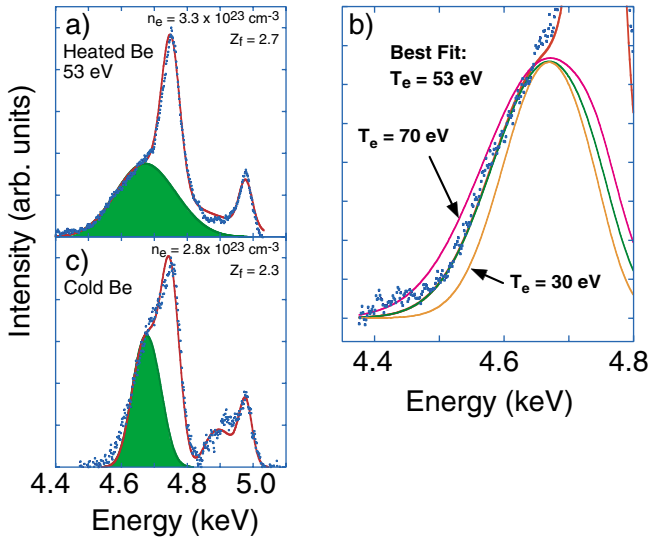

FIG. 3 (color). (a) Experimental x-ray scattering data (blue dots) from the heated Be plasma with a theoretical fit yielding $T_e = 53$ eV and $n_e = 3.3 \times 10^{23}$ cm^{-3}. (b) Red wing of the scattering spectrum together with the best fit and calculated spectra for $T_e = 30$ eV and $T_e = 70$ eV indicating that the electron temperature is determined with 10%–20% accuracy. (c) Experimental x-ray scattering data (blue dots) from the cold Be indicating $T_e \approx 2$ eV and $n_e = 2.8 \times 10^{23}$ cm^{-3}. The green shaded area corresponds to the Compton down-shifted feature as obtained from the fit.

approximation is typically valid for plasmas that are only weakly collisional and ideal; e.g., the number of electrons N_s inside a sphere of radius λ_s is large. The correlation length, λ_s, represents the screening distance of electrostatic forces; thus, the parameter $\alpha = 1/k\lambda_s$ is a measure of the importance of the electrostatic correlations as defined by the probe geometry. When $\alpha \ll 1$, the scattering is only sensitive to distances shorter than the screening length, hence denoted noncollective, which is the case in our experiments. The fit indicates $T_e = 53$ eV from the spectral shape of the red wing of the broadened Compton line in the range of 4.40 keV $< E <$ 4.67 keV. Figure 3(b) demonstrates the sensitivity of the spectra to the electron temperature by comparing calculated electron feature spectra for $T_e = 30$, 53, and 70 eV with the experiment. By varying the theoretical spectra within the noise of the data, we find that T_e can be determined with an accuracy in the range of 10%–20%.

We tested the theoretical x-ray scattering spectra of the RPA by comparing with the results in the well-known limit of zero temperature [13–16] as well as with calculated scattering spectra assuming $\alpha \ll 1$ for which the spectra directly show the distribution function [6]. Since for our conditions, the scattering regime is noncollective ($\alpha = 0.4$), we find that the results of the RPA are indistinguishable from the more conventional calculations based on assuming a scattering spectrum that reproduces the electron velocity distribution function. Moreover, for the experimental data shown in Fig. 3(a), the plasma is weakly coupled with a coupling parameter of $\Gamma \sim N_s^{-2/3} = 0.3$. At these couplings, previous experiments conducted on laboratory plasmas have shown minimal deviations from the RPA [17].

For the cold plasma conditions [shown in Fig. 3(c)], we infer a low temperature of $T_e = 2.5 \pm 2$ eV, where the plasma is in the degenerate state. In this regime with $T_e < T_F$, the electron velocity distribution transitions from the traditional temperature-dependent Gaussian Boltzmann distribution to a density-dependent parabolic Fermi distribution with a Fermi temperature of $T_F = 15$ eV for Be. In this case, the width of the Compton feature is determined by the Fermi energy [12,13], and the measured spectrum is less sensitive to electron temperature variations resulting in larger errors.

In addition to temperature measurements, the x-ray spectra provide the ratio of the inelastic scattering component to the elastic scattering component (i.e., the ratio of the electron feature to the ion feature) which is sensitive to the ionization state of the plasma. When comparing the ratio for the heated and cold Be [Figs. 3(a) and 3(c)], we find that the relative intensity of the electron feature increases with increasing temperature. This observation indicates that the number of electrons contributing to inelastic x-ray scattering increases when electrons are ionized or excited into the conduction band, e.g., giving $n_e = 3.3 \times 10^{23}$ cm^{-3} from the spectrum shown in Fig. 3(a).

Figure 4 shows the density-temperature phase diagram along with the experimental data and simulations. A third data point at $T_e = 22$ eV has been obtained from a Be target heated by Mo L-shell emission. The data set shows that spectrally resolved x-ray scattering measures for the

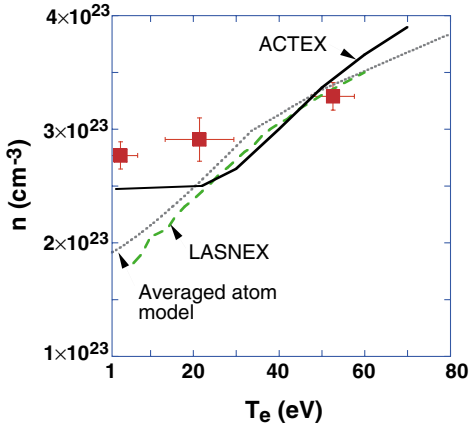

FIG. 4 (color). Density-temperature phase diagram along with the results of the x-ray scattering measurements and simulation using the ACTEX model [18], an averaged atom model [19], and radiation-hydrodynamic modeling [20]. The data and the ACTEX model include the free plus weakly bound (conduction) electrons. The averaged atom model and LASNEX only include free (ionized) electrons.

first time the microscopic properties of solid-density plasmas. We compare the experiment with calculations of the ionization balance using the activity expansion method (ACTEX) [18], with an averaged atom model [19], and with radiation-hydrodynamic calculations using the code LASNEX [20]. In the ACTEX theory, all possible interactions between the plasma constituents are calculated including the screening of the bound states. For large densities, the classical Debye-Hückel (Yukawa) potential is replaced by an expression that approaches the thermal de Broglie wavelength. This allows the calculation of delocalized electrons, i.e., the number of electrons that are no longer bound to a single ion. These electrons are free or weakly bound similar to the conduction electrons in a metal. For our conditions, these electrons give rise to the (Compton down-shifted) electron feature of the x-ray scattering spectrum.

The ion feature (Rayleigh peak) is due to scattering from tightly bound electrons. The ionization potential of these states, E_I, is larger than the Compton shift, $E_I > h^2\nu^2/m_e c^2$, which is the energy transferred by the incident x-ray photon to the electron. In this case, the tightly bound electron is neither excited nor ionized and the frequency of the scattered photon remains unchanged. Therefore, the ratio of the electron to the ion feature is a measure of the ionization balance of a solid-density plasma defined here as the ratio of the delocalized to the tightly bound electron density.

The trend of the experimental data and the ACTEX calculations is consistent; at low electron temperatures, we find that the measured density of delocalized states remains at $n_e = 2.8 \times 10^{23}$ cm^{-3} close to the calculated density of $n_e = 2.5 \times 10^{23}$ cm^{-3} corresponding to two electrons for each Be atom at $\rho = 1.85$ g/cm^{-3}. Future modeling will need to address whether the remaining deviations are due to uncertainties in the theoretical model, e.g., such as larger ion correlations than assumed in the present calculations. For comparison, the dotted curve in Fig. 4 shows modeling using an averaged atom model [19] that calculates the number of free electrons with hydrogenic wave functions. Since conduction (weakly bound) electrons are treated similar to tightly bound states, this model finds that the density falls approximately linearly for small temperatures [21]. Similarly, the radiation-hydrodynamic LASNEX calculations (dashed curve) do not distinguish between weakly and tightly bound states. LASNEX uses a model [20] that represents an interpolation between the zero and high temperature conductivity limits. For our conditions, we find that the LASNEX simulations underestimate the number of electrons that contribute to the conductivity. This shortfall of the present modeling may contribute to underestimating the electron temperature in the present simulation [cf. Fig. 1(b)]. On the other hand, for the larger temperatures, the density of electrons in the conduction band decreases and the three models agree well with the experiment.

In summary, we have demonstrated spectrally resolved x-ray scattering measurements on solid-density plasmas. The data provide accurate measurements of the plasma temperature and the ionization balance from an isochorically heated beryllium plasma testing detailed models of the electronic properties of solid-density plasmas. This novel technique has wide applications, and can access the degenerate, the closely coupled, and the ideal plasma regime. Our measurements indicate that extremely dense states of matter can be investigated such as the inertial confinement fusion fuel during compression, reaching super-solid densities.

This work was performed under the auspices of the U.S. Department of Energy by the University of California Lawrence Livermore National Laboratory under Contract No. W-7405-ENG-48. The work was supported by the Laboratory Directed Research and Development Grant No. 02-ERD-13.

[1] E. Fünfer, B. Kronast, and H.-J. Kunze, Phys. Lett. **5**, 125 (1963).
[2] H.-J. Kunze *et al.*, Phys. Lett. **11**, 42 (1964).
[3] J. J. Thomson, *Conductivity of Electricity through Gases* (Cambridge University Press, Cambridge, England, 1906).
[4] N. J. Peacock *et al.*, Nature (London) **224**, 448 (1968).
[5] S. H. Glenzer *et al.*, Phys. Plasmas **6**, 2117 (1998).
[6] O. L. Landen *et al.*, J. Quant. Spectrosc. Radiat. Transfer **71**, 465 (2001).
[7] D. Riley *et al.*, Phys. Rev. Lett. **84**, 1704 (2000).
[8] J. M. Soures *et al.*, Fusion Technol. **30**, 492 (1996).
[9] F. J. Marshall and J. A. Oertel, Rev. Sci. Instrum. **68**, 735 (1997).
[10] B. Yaakobi and A. J. Burek, J. Quantum Electron. **19**, 1841 (1983).
[11] A. H. Compton, Phys. Rev. **21**, 483 (1923).
[12] J. W. M. DuMond, Phys. Rev. **29**, 643 (1929).
[13] S. Chandrasekhar, Proc. R. Soc. London A **125**, 231 (1929).
[14] G. Gregori *et al.*, Phys. Rev. E **67**, 026413 (2003).
[15] D. Pines and P. Nozieres, *The Theory of Quantum Fluids* (Addison-Wesley, Redwood, CA, 1990).
[16] J. Chihara, J. Phys. Condens. Matter **12**, 231 (2000).
[17] H. Röhr, Z. Phys. **209**, 295 (1968).
[18] F. J. Rogers, Phys. Plasmas **7**, 51 (2000); F. J. Rogers and D. A. Young, Phys. Rev. E **56**, 5876 (1997).
[19] O. Peyrusse, J. Quant. Spectrosc. Radiat. Transfer **43**, 397 (1990).
[20] M. P. Desjarlais, J. D. Kress, and L. A. Collins, Phys. Rev. E **66**, 025401 (2002); M. P. Desjarlais, Contrib. Plasma Phys. **41**, 267 (2000).
[21] In addition to the averaged atom model, the author of Ref. [19] also calculates the total x-ray scattering cross section, but provides no explicit expression of the relative contribution of the weakly and tightly bound electrons. In the future, it will be interesting to compare the present data with such calculations.